

High performance liquid crystal displays with a low dielectric constant material

Haiwei Chen,¹ Fenglin Peng,¹ Zhenyue Luo,¹ Daming Xu,¹ Shin-Tson Wu,^{1*}
Ming-Chun Li,² Seok-Lyul Lee,² and Weng-Ching Tsai²

¹College of Optics and Photonics, University of Central Florida, Orlando, Florida 32816, USA

²AU Optronics Corp., Hsinchu Science Park, Hsinchu 300, Taiwan

*swu@ucf.edu

Abstract: We report high performance liquid crystal displays (LCDs), including fringe field switching (p-FFS) and in-plane switching (p-IPS), with a small average dielectric constant (ϵ) but positive dielectric anisotropy material. Our low ϵ based p-FFS and p-IPS LCDs offer several attractive properties, such as high transmittance, low operation voltage, fast response time (even at -20°C), which is particularly desirable for outdoor applications of mobile or wearable display devices, and suppressed flexoelectric effect. Combining these advantages with the inherent outstanding features, such as wide viewing angle, no grayscale inversion, negligible color shift, and pressure resistance, the low ϵ LC based p-FFS and p-IPS are strong contenders for next-generation mobile displays, and high resolution and high frame rate TVs.

©2014 Optical Society of America

OCIS codes: (160.3710) Liquid crystals; (230.3720) Liquid-crystal devices.

References and links

1. M. Schadt, "Milestone in the history of field-effect liquid crystal displays and materials," *Jpn. J. Appl. Phys.* **48**, 03B001 (2009).
2. Y. Takubo, Y. Hisatake, T. Iizuka, and T. Kawamura, "Ultra-high resolution mobile displays," *SID Symp. Dig.* **64**, 869–872 (2012).
3. M. Emoto, Y. Kusakabe, and M. Sugawara, "High-frame-rate motion picture quality and its independence of viewing distance," *J. Display Technol.* **10**(8), 635–641 (2014).
4. S. H. Lee, S. L. Lee, and H. Y. Kim, "Electro-optic characteristics and switching principle of a nematic liquid crystal cell controlled by fringe-field switching," *Appl. Phys. Lett.* **73**(20), 2881–2883 (1998).
5. S. H. Lee, H. Y. Kim, S. M. Lee, S. H. Hong, J. M. Kim, J. W. Koh, J. Y. Lee, and H. S. Park, "Ultra-FFS TFT-LCD with super image quality, fast response time, and strong pressure-resistant characteristics," *J. Soc. Inf. Disp.* **10**(2), 117–122 (2002).
6. H. J. Yun, M. H. Jo, I. W. Jang, S. H. Lee, S. H. Ahn, and H. J. Hur, "Achieving high light efficiency and fast response time in fringe field switching mode using a liquid crystal with negative dielectric anisotropy," *Liq. Cryst.* **39**(9), 1141–1148 (2012).
7. Y. Chen, F. Peng, T. Yamaguchi, X. Song, and S. T. Wu, "High performance negative dielectric anisotropy liquid crystals for display applications," *Crystals* **3**(3), 483–503 (2013).
8. Y. Chen, Z. Luo, F. Peng, and S. T. Wu, "Fringe-field switching with a negative dielectric anisotropy liquid crystal," *J. Display Technol.* **9**(2), 74–77 (2013).
9. M. Schadt, K. Schmitt, V. Kozinkov, and V. Chigrinov, "Surface-induced parallel alignment of liquid crystals by linearly polymerized photopolymers," *Jpn. J. Appl. Phys.* **31**(Part 1), 2155–2164 (1992).
10. L. Rao, S. Gauza, and S. T. Wu, "Low temperature effects on the response time of liquid crystal displays," *Appl. Phys. Lett.* **94**(7), 071112 (2009).
11. I. Haller, "Thermodynamic and static properties of liquid crystals," *Prog. Solid State Chem.* **10**, 103–118 (1975).
12. S. T. Wu, "Birefringence dispersions of liquid crystals," *Phys. Rev. A* **33**(2), 1270–1274 (1986).
13. W. H. De Jeu, "Physical properties of liquid crystalline materials in relation to their applications," *Mol. Cryst. Liq. Cryst. (Phila. Pa.)* **63**(1), 83–109 (1981).
14. S. T. Wu and C. S. Wu, "Rotational viscosity of nematic liquid crystals A critical examination of existing models," *Liq. Cryst.* **8**(2), 171–182 (1990).
15. S. T. Wu and C. S. Wu, "Experimental confirmation of the Osipov-Terentjev theory on the viscosity of nematic liquid crystals," *Phys. Rev. A* **42**(4), 2219–2227 (1990).
16. W. Maier, A. Saupe, and Z. Naturforsch, Teil A **14**, 882 (1959). **15**, 287 (1960).

17. J. W. Ryu, J. Y. Lee, H. Y. Kim, J. W. Park, G. D. Lee, and S. H. Lee, "Effect of magnitude of dielectric anisotropy of a liquid crystal on light efficiency in the fringe-field switching nematic liquid crystal cell," *Liq. Cryst.* **35**(4), 407–411 (2008).
18. S. W. Kang, I. W. Jang, D. H. Kim, Y. J. Lim, and S. H. Lee, "Enhancing transmittance of fringe-field switching liquid crystal device by controlling perpendicular component of dielectric constant of liquid crystal," *Jpn. J. Appl. Phys.* **53**(1), 010304 (2014).
19. A. Lien, "Extended Jones matrix representation for the twisted nematic liquid-crystal display at oblique-incidence," *Appl. Phys. Lett.* **57**(26), 2767–2769 (1990).
20. Z. Ge, X. Zhu, T. X. Wu, and S. T. Wu, "High transmittance in-plane- switching liquid crystal displays," *J. Display Technol.* **2**(2), 114–120 (2006).
21. C. D. Tu, C. L. Lin, J. Yan, Y. Chen, P. C. Lai, and S. T. Wu, "Driving scheme using bootstrapping method for blue-phase LCDs," *J. Display Technol.* **9**(1), 3–6 (2013).
22. Y. Iwata, M. Murata, K. Tanaka, T. Ohtake, H. Yoshida, and K. Miyachi, "Novel super fast response vertical alignment-liquid crystal display with extremely wide temperature range," *J. Soc. Inf. Disp.* **10**, 1002–1019 (2014).
23. L. M. Blinov and V. G. Chigrinov, *Electrooptic Effects In Liquid Crystal Materials* (Springer-Verlag, 1994).
24. Z. Luo, D. Xu, and S. T. Wu, "Emerging quantum-dots-enhanced LCDs," *J. Display Technol.* **10**(7), 526–539 (2014).
25. C. H. Oh, H. M. Moon, W. K. Yoon, J. H. Kim, M. H. Song, J. J. Kim, J. H. Lee, J. H. Kim, C. S. Im, S. W. Lee, H. C. Choi, and S. D. Yeo, "Super-large-sized TFT-LCD (55 in.) for HDTV application," *J. Soc. Inf. Disp.* **12**(1), 11–16 (2004).
26. R. Lu, Q. Hong, S. T. Wu, K. H. Peng, and H. S. Hsieh, "Quantitative comparison of color performances between IPS and MVA LCDs," *J. Display Technol.* **2**(4), 319–326 (2006).
27. Y. Igarashi, T. Yamamoto, Y. Tanaka, J. Someya, Y. Nakakura, M. Yamakawa, Y. Nishida, and T. Kurita, "Summary of moving picture response time (MPRT) and futures," *SID Symp. Dig.* **35**, 1262–1265 (2004).
28. J.-K. Yoon, E.-M. Park, J.-S. Son, H.-W. Shin, H.-E. Kim, M. Yee, H.-G. Kim, C.-H. Oh, and B.-C. Ahn, "The study of picture quality of OLED TV with WRGB OLEDs structure," *SID Symp. Dig.* **44**, 326–329 (2013).
29. K. H. Kim and J. K. Song, "Technical evolution of liquid crystal displays," *Npg Asia Mater.* **1**(1), 29–36 (2009).
30. M. Oh-e and K. Kondo, "Electro-optical characteristics and switching behavior of the in-plane switching mode," *Appl. Phys. Lett.* **67**(26), 3895–3897 (1995).

1. Introduction

Thin film transistor liquid crystal displays (TFT-LCDs) are ubiquitous nowadays; their applications span from smartphones, pads, computer screens, to TVs. Some commonly desired features of an LCD include low power consumption (low voltage and high transmittance), wide view, unnoticeable color shift, and fast response time [1]. Recently, high resolution [e.g. 4K2K (3840X2160) or 8K4K (7680X4320)] and high frame rate (≥ 120 Hz) LCDs are emerging because of the strong demand for crisp and clear images [2, 3]. However as the resolution density and frame rate increase, high transmittance and fast LC response time become critically important. High transmittance helps to reduce power consumption, whereas fast response time and high frame rate mitigate image blurs. For mobile devices, wearable displays, or car navigation system, fast response time at low temperatures is particularly important.

Fringe field switching (FFS) LCD has been widely used in mobile displays because of its outstanding features like high transmittance, wide view, weak color shift, and pressure resistance for touch panels [4–6]. Both positive and negative $\Delta\epsilon$ LC mixtures can be used for FFS [6–8]. Presently, positive FFS (p-FFS) mode dominates because of its low operation voltage, no grayscale inversion, and no image sticking with commercial photoalignment materials [9], regardless its peak transmittance is $\sim 10\%$ lower than that of n-FFS [6,8]. However, the response time of n-FFS is about 2-3x slower than that of p-FFS. For TV applications, p-FFS has a slower response time than its multi-domain vertical alignment (MVA) competitor because the involved elastic constant (K) is different. MVA utilizes bend elastic constant (K_{33}) while FFS mainly uses twist elastic constant (K_{22}), and in general K_{33} is $\sim 2\text{-}3\text{x}$ larger than K_{22} . Presently, MVA is dominating TV market because of its higher contrast ratio and faster response time. However, MVA is not ideal for touch panels because of its poor pressure resistance. In order to enable p-FFS for high resolution TV applications, there is urgent need to improve its response time while keeping high transmittance.

To overcome the above mentioned problems, in this paper, we find that p-FFS with a low average dielectric constant [$\varepsilon = (\varepsilon_{//} + 2\varepsilon_{\perp})/3$] LC can offer a complete solution. Such a p-FFS LCD exhibits several outstanding features: high transmittance (>90%) at 5V operation voltage, fast response time (even at -20°C), suppressed flexoelectric effect, and large tolerance to electrode gap variation. Therefore, it is a strong contender for next-generation high resolution and high frame rate TVs, mobile devices, and wearable displays.

2. Experiment

To prove concept, in experiment we prepared a low ε LC mixture (called UCF-L1) consisting of 80% SLC-UCF-01 (a low viscosity mixture reported in [10]) and 20% 5PP3 (P stands for phenyl ring, and 5 and 3 are the carbon numbers of alkyl chains) as a diluter to further reduce the viscosity and dielectric anisotropy. We compare the electro-optic properties of UCF-L1 with Merck MLC-6686 (a benchmark mixture for p-FFS). Table 1 lists the physical properties of these two mixtures. MLC-6686 has a relatively large dielectric anisotropy [$\Delta\varepsilon = \varepsilon_{//} - \varepsilon_{\perp}$] so that its operation voltage is low. However, a tradeoff is its high viscosity because more polar groups are involved. On the other hand, UCF-L1 has a small ε . Please note that a small $\Delta\varepsilon$ does not necessarily lead to small ε ; but the reverse is true. The major attraction of low ε LC is its ultra-low rotational viscosity. One drawback of UCF-L1 is its low clearing point $T_c = 60^{\circ}\text{C}$, which is too low for practical applications. Nevertheless, it serves as an important example for elucidating the key features of our proposed low ε materials.

Table 1. Physical properties of two LC mixtures studied ($T = 23^{\circ}\text{C}$, $\lambda = 633\text{nm}$ and $f = 1$ kHz.)

LC	Δn	$\varepsilon_{//}$	ε_{\perp}	ε	γ_1 (mPa·s)	K_{11} (pN)	K_{22} (pN)	T_c ($^{\circ}\text{C}$)
MLC-6686	0.097	14.50	4.50	7.83	102	8.8	6.7	71
UCF-L1	0.121	5.65	2.76	3.72	35	10.2	5.5	60

2.1 Temperature dependent birefringence

Birefringence (Δn) affects the cell gap (d), which in turn affects response time. We measured the temperature dependent Δn of UCF-L1 and MLC-6686 at $\lambda = 633$ nm using a commercial homogeneous cell with $d = 5$ μm . Results are shown in Fig. 1, where dots stand for measured data and red line for the fitting results using Haller's semi-empirical equation [11, 12]:

$$\Delta n(T) = \Delta n_0 S = \Delta n_0 (1 - T / T_c)^{\beta}, \quad (1)$$

where Δn_0 is the extrapolated birefringence at $T = 0$, S is the order parameter, T is the temperature, T_c is the clearing point, and β is a material parameter. Through fittings, we obtained $\Delta n_0 = 0.187$ and $\beta = 0.191$ for UCF-L1, and $\Delta n_0 = 0.137$ and $\beta = 0.200$ for MLC-6686. Using these fitting parameters, we can calculate the order parameter (S), which will be used later.

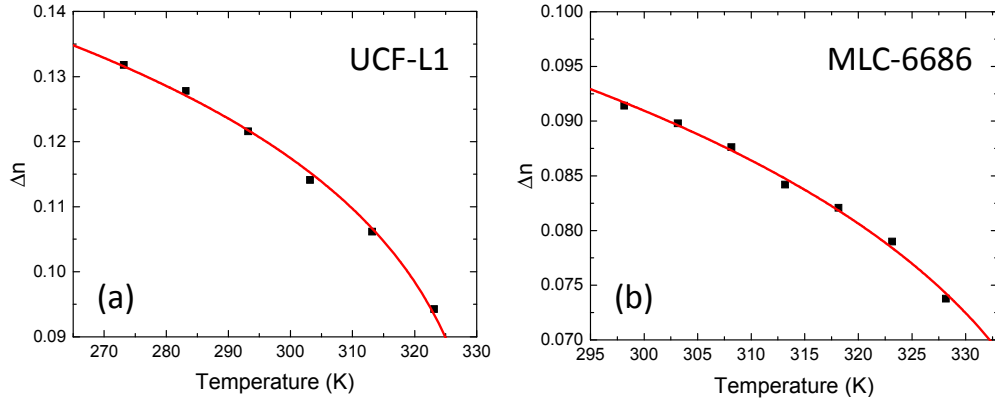


Fig. 1. Temperature dependent birefringence of (a) UCF-L1 and (b) MLC-6686 at $\lambda = 633\text{nm}$. Dots are experimental data and red line is fitting curve with Eq. (1).

2.2 Temperature dependent visco-elastic constant

In a FFS cell, the electric field is not uniform; it contains both longitudinal and lateral components. Thus, it is not easy to derive the analytical expression for the LC response time because both K_{11} and K_{22} are involved. Therefore, we measured the response time of UCF-L1 and MLC-6686 using FFS cells with photoalignment, cell gap $d = 3.5\mu\text{m}$, electrode width $w = 4\mu\text{m}$, electrode gap $l = 3\mu\text{m}$, and rubbing angle $\varphi = 7^\circ$. Figure 2 shows the measured data.

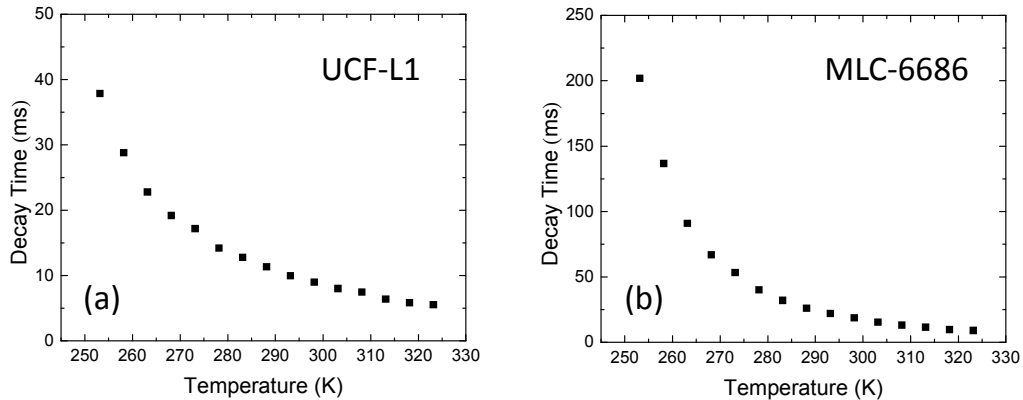


Fig. 2. Measured decay time of (a) UCF-L1 and (b) MLC-6686. FFS cell: $d = 3.5\mu\text{m}$, $w = 4\mu\text{m}$, and $l = 3\mu\text{m}$.

From Fig. 2, the response time of both MLC-6686 and UCF-L1 increases as the temperature decreases, but at different rates. For example, at $T = 25^\circ\text{C}$ the decay time of MLC-6686 is only $\sim 2\times$ slower than that of UCF-L1, but this ratio jumps to 6 at -20°C . The slower response time at lower temperature is easy to understand because the rotational viscosity increases exponentially as [13, 14]:

$$\gamma_1 \sim S \cdot \exp(E / k_B T), \quad (2)$$

where E is the activation energy and k_B the Boltzmann constant. From Eq. (2), activation energy plays a key role affecting the rising rate of rotational viscosity in the low temperature region. Key parameters affecting activation energy include molecular structure and conformation, and intermolecular interactions [15]. A low ϵ LC mixture mainly consists of weakly polar and non-polar low molecular weight compounds. As a result, its activation energy is relatively small, which in turn causes a mild increase as the temperature decreases.

To validate this hypothesis, we measured the visco-elastic coefficient of UCF-L1 and MLC-6686 using commercial homogeneous cells with $d = 5 \mu\text{m}$. In a homogeneous cell, the electric field is uniform and the response time is proportional to γ_l/K_{11} ; here K_{11} is the splay elastic constant. In theory, temperature dependent γ_l/K_{11} can be described as follows [13–16]:

$$K_{ii} \sim S^2, \quad (3)$$

$$\gamma_l / K_{ii} \sim \exp(E / k_B T) / S, \quad (4)$$

where K_{ii} is the corresponding elastic constant which depends on the LC alignment (e.g. $K = K_{33}$ for a VA cell).

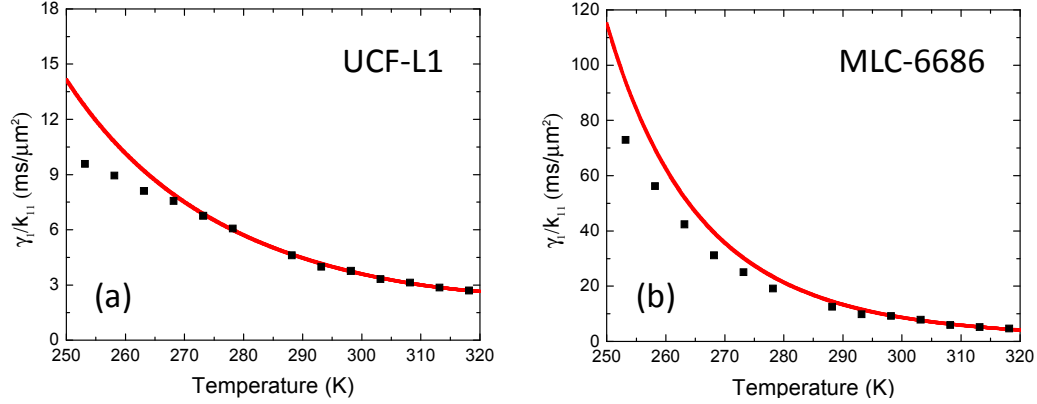


Fig. 3. Temperature dependent γ_l/K_{11} of (a) UCF-L1 and (b) MLC-6686: black dots are experimental data and red lines are fittings with Eq. (4).

Figures 3(a) and 3(b) depict the measured data (black dots) and fitted curves (red solid lines) for UCF-L1 and MLC-6686, respectively. In the high temperature region, the experimental data fit well with Eq. (4). However, noticeable deviation is observed in the low temperature region. Similar phenomenon has been observed by Rao *et al.* [10]. In the low temperature region, K_{11} no longer follows Eq. (3); it is larger than expected, resulting in a smaller γ_l/K_{11} . At -20°C the measured γ_l/K_{11} is $\sim 30\%$ lower than the fitted result through Eq. (4). The activation energy we obtained through fitting is $E = 199.7 \text{ meV}$ for UCF-L1, which is much smaller than that of MLC-6686 ($E = 353.9 \text{ meV}$). Because UCF-L1 has small activation energy, its response time is much less sensitive to the temperature change, as Fig. 2 depicts.

2.3 Voltage-Transmittance curves

We used the same FFS cell described above to measure the voltage-dependent transmittance (VT) curves for both mixtures at $\lambda = 633\text{nm}$. Results are shown in Fig. 4. Good agreement between experiment (dashed lines) and simulation (solid lines) is found. From Fig. 4, the peak transmittance of UCF-L1 is much higher than that of MLC-6686 (88% vs. 73%), albeit the on-state voltage is 2V higher. The enhanced transmittance mainly results from lower $\Delta\epsilon$ [17] and higher $\epsilon_{\perp}/\epsilon_{\parallel}$ ratio [18] of UCF-L1. Detailed explanation will be given in Sec. 3.3. As $\Delta\epsilon$ decreases, both on-state voltage and peak transmittance increase. Therefore, a delicate balance between low voltage and high transmittance should be taken into consideration.

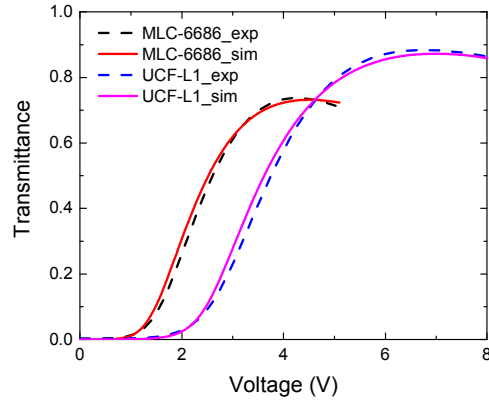


Fig. 4. Measured and simulated VT curves for UCF-L1 and MLC-6686. FFS cell: $d = 3.5\mu\text{m}$, $\omega = 4\mu\text{m}$, and $l = 3\mu\text{m}$. $\lambda = 633\text{ nm}$.

3. Simulation

To optimize the device performance, we simulate the electro-optic properties of p-FFS cell employing UCF-L1 with a commercial LCD simulator DIMOS.2D and the extended 2×2 Jones matrix method [19]. In order to achieve high transmittance and low operation voltage, we set $d\Delta n \sim 380\text{nm}$ according to Ref [8]. The corresponding cell gap is $d = 3.08\mu\text{m}$ and $3.86\mu\text{m}$ for UCF-L1 and MLC-6686, respectively. To make a fair comparison, we use the same cell parameters during simulations: electrode width $w = 2\mu\text{m}$, electrode gap $l = 3\mu\text{m}$, pretilt angle $\theta_p = 2^\circ$ and rubbing angle $\varphi = 10^\circ$. The passivation layer between pixel and common electrode is SiO_2 whose thickness $d_p = 250\text{nm}$ and dielectric constant is $\epsilon_p = 4.5$ [20]. The cell is sandwiched between two crossed linear polarizers, and the transmission axis of bottom polarizer is parallel to the rubbing direction.

3.1 VT curves

Figure 5 depicts the simulated VT curves of p-FFS cells employing UCF-L1 and MLC-6686. UCF-L1 has a smaller $\Delta\epsilon$ so that its operation voltage is higher than that of MLC-6686 (6.2V vs. 5.2V) [17]. However, its peak transmittance is $\sim 95.1\%$, which is comparable to that of n-FFS [6, 8]. The transmittance can be further improved to $\sim 98\%$ by optimizing $\epsilon_{//}$ and ϵ_{\perp} (Sec. 3.3). From Fig. 5, if we are willing to sacrifice 4% in transmittance, then we can drive the p-FFS cell at 5V and obtain the same transmittance ($\sim 91\%$) as MLC-6686.

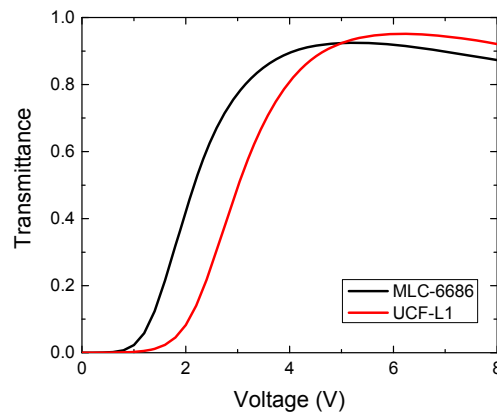


Fig. 5. Simulated VT curves of MLC-6686 and UCF-L1. $\lambda = 550\text{ nm}$.

The power consumption of a LCD originates from two parts: electrical and optical. For a small-sized display like smartphone, these two parts are roughly equal. As the panel size increases, the backlight part gradually dominates. For example, in a 50" LCD TV the backlight consumes ~90% of the total power. The electrical power consumption (P) of the display part can be characterized by:

$$P \sim N \cdot f \cdot C \cdot V^2, \quad (5)$$

where N is the total number of pixels, f is the frame rate, C is the capacitance, and V is the driving voltage. In a TFT-LCD, the storage capacitor (C_{st}) and LC capacitor (C_{lc}) are connected in parallel. Therefore, the total capacitance is:

$$C = C_{st}(1 + C_{lc} / C_{st}). \quad (6)$$

In a nematic LCD, C_{lc} is 5x-10x smaller than C_{st} . Thus, the second term (C_{lc} / C_{st}) in Eq. (6) is small. Both power consumption and pixel charging time are primarily determined by the storage capacitor. However, in a polymer-stabilized blue phase LCD, C_{lc} could be very large and the second term cannot be neglected [21]. This increases the pixel's charging time and power consumption.

3.2 Response time

Another major advantage of such a small ϵ LC material is its ultra-low viscosity. From Table 1, the rotational viscosity of UCF-L1 is only 35 mPa·s. In contrast, the rotational viscosity of MLC-6686 is 102 mPa·s, which is nearly 3x higher. To obtain a large $\Delta\epsilon$ LC such as MLC-6686, multiple dipole groups are needed, which leads to substantially increased viscosity.

We calculated the turn-on and turn-off times from the time-dependent transmittance curves shown in Fig. 6. As usual, the response time is defined as 10%–90% transmittance change. For MLC-6686, the simulated response time [rise, decay] is [26.2ms, 29.6ms] at $V_{on} = 5.2V$, whereas the response time of UCF-L1 is [6.5ms, 7.8ms] at $V_{on} = 6.2V$. The ~4x faster response time of UCF-L1 originates from its lower viscosity and thinner cell gap (3.08 μm vs. 3.87 μm). Also from Fig. 6, fast response time improves transmittance (the area covered by the red line) and fast decay time reduces image crosstalk.

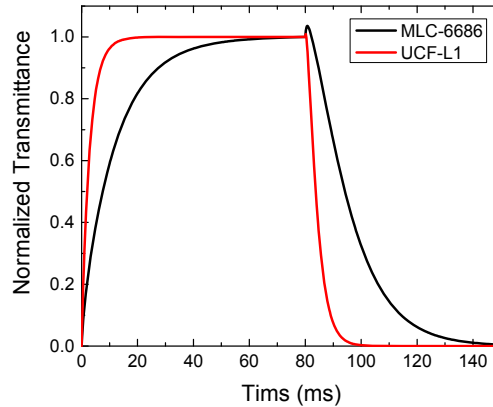


Fig. 6. Simulated response time for UCF-L1 and MLC-6686.

To evaluate the gray-to-gray (GTG) response time, in simulations we divided the VT curve uniformly into 8 gray levels (1-8). Table 2 summarizes the GTG rise and decay times of the p-FFS cell using UCF-L1. The averaged GTG response time [rise time, decay time] is [9.4ms, 9.8ms]. Such a response time is comparable to that of MVA [22]. This enables p-FFS to be used for TV applications.

Table 2. Simulated gray-to-gray response time for UCF-L1 (ms).

	1	2	3	4	5	6	7	8
1		16.4	15.3	13.9	12.3	11.5	9.5	6.5
2	6.3		11.8	11.6	10.7	10.1	8.4	5.7
3	6.4	12.0		10.7	10.5	9.9	8.3	5.5
4	6.6	11.8	9.5		9.3	9.1	8.3	5.7
5	6.8	11.7	9.2	8.9		9.0	7.3	5.9
6	7.2	11.8	9.7	9.3	8.3		7.2	6.2
7	7.4	11.8	11.5	11.2	10.6	9.2		6.9
8	7.8	12.2	12.5	12.2	11.5	11.5	9.9	

For outdoor applications of LCD devices, the slow response time at low temperature causes severe image blurs [22]. From Eq. (2), the rotational viscosity increases exponentially as the temperature decreases. However, UCF-L1 has fairly small activation energy ($E \sim 200$ meV) so that its rotational viscosity in the low temperature region remains relatively low. From Fig. 2, the measured decay time at -20°C is 37 ms for the $3.5\text{-}\mu\text{m}$ cell gap employed. If we use the optimized cell gap $3.08\text{ }\mu\text{m}$, the response time should be ~ 28 ms. This is still relatively fast at such a low temperature. As reported in [22], the rise time (from 0 to 32nd grayscale without overdrive) of a MVA at -20°C is as sluggish as 1000 ms.

3.3 Dielectric constant effect

The operation voltage of p-FFS mode is inversely proportional to the square root of $\Delta\epsilon$ [17]. Here, we investigate the influence of $\epsilon_{//}$ and ϵ_{\perp} on the electro-optic performance of p-FFS. First, let us keep $\epsilon_{\perp} = 2.76$ and vary $\epsilon_{//}$. Figure 7(a) shows that the operation voltage decreases from 6.2V to 4.6V when $\epsilon_{//}$ increases from 5.65 to 9.65. Meanwhile, the transmittance decreases from 95.1% to 86.7% owing to the effect of ϵ_{\perp} , as will be discussed later.

If we keep $\Delta\epsilon = 2.89$ while gradually increasing ϵ_{\perp} , we find that the operation voltage remains unchanged (Fig. 7(b)), but the peak transmittance is improved. These results are consistent with those reported in [18]. Figure 7(c) illustrates this trend more clearly: the operation voltage keeps the same, while the transmittance increases from 91.1% to 97.9% with the increasing $\epsilon_{\perp}/\epsilon_{//}$ ratio. It means increasing ϵ_{\perp} helps boost the transmittance. The detailed explanation has been given in [18]. Here we just emphasize that high transmittance ($\sim 98\%$) and relatively low voltage can be achieved by optimizing $\epsilon_{//}$ and ϵ_{\perp} .

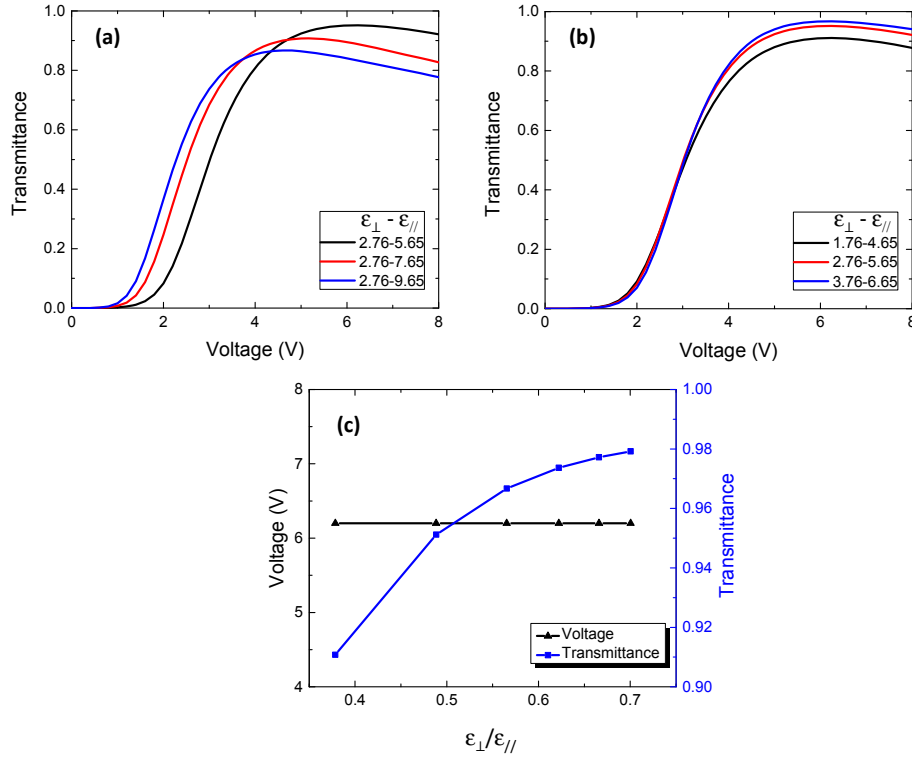


Fig. 7. Simulated VT curves for different (a) ϵ_{\perp} , (b) ϵ_{\perp} , and (c) $\epsilon_{\perp}/\epsilon_{\parallel}$. $\lambda = 550$ nm.

3.4 Electrode structure effect

When the electrode gap increases, the voltage of p-FFS would decrease because of more horizontal electric fields are generated between electrodes, as shown in Fig. 8(a) [4]. The on-state voltage of MLC-6686 decreases from 5.2V to 4.6V as the electrode gap (l) increases from $3\mu\text{m}$ to $4\mu\text{m}$ while keeping the electrode width at $w = 2\mu\text{m}$. However, as Fig. 8(b) depicts the on-state voltage of UCF-L1 only decreases slightly from 6.2V to 6.0V, which is less sensitive to the electrode gap variation. The reason is that low $\Delta\epsilon$ material is less sensitive to electric fields. As a result, UCF-L1 offers a larger tolerance for electrode fabrication.

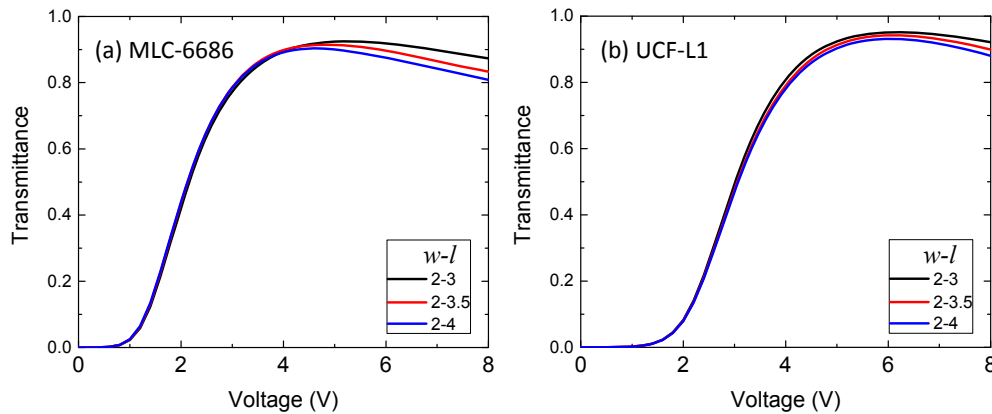


Fig. 8. Simulated VT curves for different electrode structures of (a) MLC-6686 and (b) UCF-L1. $\lambda = 550$ nm.

3.5 Flexoelectric effect

Because of the non-uniform electric field, the splay deformation would occur in p-FFS and electric polarization is induced, which is known as flexoelectric effect [23]. The light transmittance would differ from negative to positive frames, resulting in a small image flickering. For the low $\Delta\epsilon$ material, the tilt angle is less sensitive to the electric field, which in turn results in weaker splay deformation [Fig. 9(a)]. But for a large $\Delta\epsilon$ LC (e.g. MLC-6686), LC directors near the middle of electrodes and gaps tilt at a large angle [Fig. 9(b)]. Therefore, low $\Delta\epsilon$ material has an extra built-in advantage, which is suppressed flexoelectric effect. In addition, the large tilt angle caused by the strong vertical field [Fig. 9(b)] reduces the effective birefringence and hence the peak transmittance is lower [8].

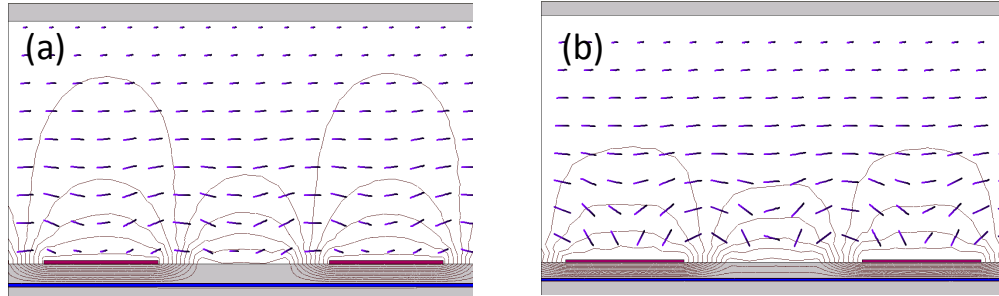


Fig. 9. LC director deformation of (a) UCF-L1, and (b) MLC-6686.

4. Discussion

To enable widespread applications, the proposed low ϵ LC materials have to compete with the state-of-the-art LCDs. Although the ultra-low viscosity is highly favorable for fast response time, especially at low ambient temperature, its small $\Delta\epsilon$ could lead to high operation voltage. Therefore, a delicate balance between these two parameters should be taken into consideration. Fortunately, the operation voltage is inversely proportional to the square-root of $\Delta\epsilon$. Moreover, the p-FFS using such a low ϵ LC exhibits >95% transmittance because of the small tilt angle [Fig. 9(a)]. As Fig. 5 shows, we can still obtain 91% transmittance at 5V. Thus, the disadvantage in operation voltage can be mitigated while the advantage in fast response time remains.

4.1 Comparison with n-FFS

For mobile displays, we have to compare our low ϵ based p-FFS with the emerging n-FFS mode [6,7]. Here we summarize the advantages of our low ϵ based p-FFS mode: 1) its peak transmittance (Fig. 5) is comparable to that of n-FFS. 2) The single-domain n-FFS exhibits grayscale inversion at large viewing angles [24], but p-FFS does not. 3) The image sticking problem of p-FFS using commercial photoalignment materials (for high resolution density displays) has been solved, but it remains a challenge for n-FFS. And 4) the response time of our p-FFS is $\sim 4x$ faster than that of n-FFS. This feature is particularly important for low temperature operation of mobile devices. Our estimated response time of p-FFS using UCF-L1 is about 28 ms at -20°C .

4.2 Comparison with MVA

For TV applications, we have to compare our low ϵ based p-FFS with the presently dominating MVA mode. Indeed, MVA offers a higher contrast ratio (5000:1) than p-FFS ($\sim 2000:1$), but only in the $\sim 20^\circ$ viewing cone [25]. Outside this cone, FFS is actually better. Our low ϵ based p-FFS offers following key advantages over MVA: 1) p-FFS has a much weaker color shift than MVA [24, 26]. 2) When zigzag structure (for wide view) is

considered, p-FFS has a higher transmittance (85% vs. 75%) than MVA. And 3) its response time in the low temperature region is much faster because of its smaller activation energy.

In addition to higher transmittance [Fig. 6], fast response time of p-FFS also plays a key role for reducing the motion image blurs. Motion blur is often characterized by motion picture response time (MPRT), which is affected both by LC response time and TFT sample-and-hold (S&H) effect [27]. As the frame rate increases from 60 Hz to 120 Hz, the motion blur is dramatically improved; but further increasing frame rate to 240 Hz and 480 Hz, the effect gradually saturates [3]. Although boosting frame rate is an effective approach to suppress image blurs, it requires faster TFT charging time and LC response time, and moreover it increases electronic power consumption as Eq. (5) indicates. Therefore, the sweet spot is in the 120Hz-240Hz range. According to a recent study [28], at 120Hz frame rate a LCD with 5.69ms GTG response time corresponds to MPRT~7.56ms, while an OLED TV with 0.1ms GTG material response time only shows a slightly faster MPRT~6.65ms. If we increase the frame rate to 240Hz while reducing the LC response time to 3.84ms, the MPRT is 5.40ms, which means the displayed image is clearer than that of OLED operated at 120Hz. Our low ε and ultra-low viscosity LC material significantly decreases the response time of p-FFS mode and enables high frame rate. By combining 120Hz frame rate driving with blinking (scanning) backlight or black image insertion [29], the motion blurs can be further suppressed.

For a large-screen LCD TV, the major power consumption is from backlight. Therefore, we can tolerate a slightly higher operation voltage, say 10V. This is particularly favorable for our low ε LC materials because low ε leads to a small $\Delta\varepsilon$. Here, we explore the lower limit of $\Delta\varepsilon$. As Fig. 7 shows, the peak transmittance depends on $\Delta\varepsilon$ and $\varepsilon_{\perp}/\varepsilon_{\parallel}$. For simplicity, we keep $\Delta n = 0.123$, $\varepsilon_{\perp} = 2.76$, and same p-FFS device configuration, while varying $\Delta\varepsilon$. The simulated results are plotted in Fig. 10.

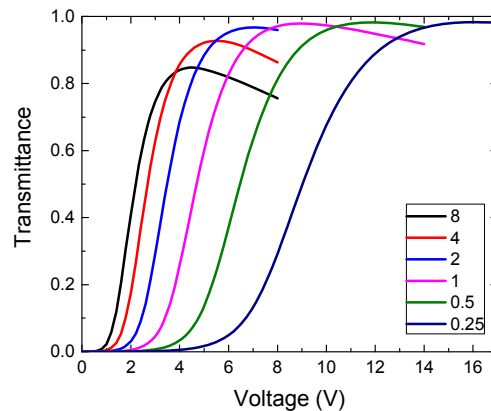


Fig. 10. Simulated VT curves of p-FFS as $\Delta\varepsilon$ decreases from 8.0 to 0.25. $\lambda = 550$ nm and $\varepsilon_{\perp} = 2.76$.

From Fig. 10, as $\Delta\varepsilon$ decreases from 8 to 0.25, the peak transmittance gradually increases from 84.8% and finally saturates at 98.4%, but the on-state voltage increases from 4.4V to 16V. It is amazing to see from Fig. 10 that even $\Delta\varepsilon$ is as small as 1 (pink line), the on-state voltage is only 9V, which is still acceptable for TV applications. Such a low ε LC material ($\varepsilon \sim 3.09$) is expected to have ultra-low viscosity for fast response time and high frame rate.

4.3 In-Plane Switching (IPS)

As the LCD panel size increases, the pixel size increases accordingly, if we keep the same pixel density. In FFS mode, larger pixel area leads to a larger storage capacitor. Under such circumstance, the charging time could become an issue for amorphous silicon (a-Si) TFT. To

overcome this problem, we can either use high mobility oxide-semiconductor TFT or change the LC cell structure from FFS to IPS.

IPS [30] exhibits similar features to FFS, except for a slightly lower transmittance. IPS does not have a built-in storage capacitor, i.e. its storage capacitor and LC capacitor are decoupled. Therefore, we can optimize the storage capacitance for large screen TVs. Here we also investigate the electro-optic performances of IPS mode (p-IPS) using a low ϵ LC mixture. The cell parameters are kept the same as p-FFS, but without the passivation layer. From Fig. 11, both transmittance and voltage increase gradually as $\Delta\epsilon$ decreases, which is similar to p-FFS. When $\Delta\epsilon = 2$, high transmittance (90.5%) and relatively low voltage (7.2V) are achieved. With such a low ϵ , the response time should be fast as discussed above, for suppressing the image blurs, especially in the low ambient temperature.

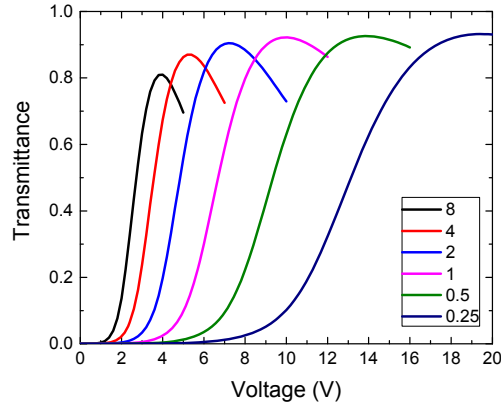


Fig. 11. Simulated VT curves of p-IPS as $\Delta\epsilon$ decreases from 8.0 to 0.25. $\lambda = 550$ nm and $\epsilon_{\perp} = 2.76$.

5. Conclusion

We have investigated the electro-optic performance of p-FFS and p-IPS LCDs using a low ϵ LC material. Such a low ϵ LC material exhibits several attractive properties: ultra-low viscosity and small activation energy, high transmittance, and weak flexoelectric effect. The ultra-low viscosity originates from the weak-polar and non-polar short-chain and low molecular weight LC compositions. The small activation energy (200 meV) of UCF-L1 keeps the response time relatively fast (<30 ms) even at -20°C . This is particularly desirable for the outdoor application of mobile or wearable displays. A major concern of the low ϵ LC material is its potentially high operation voltage. However, the operation voltage is inversely proportional to the square-root of $\Delta\epsilon$. Moreover, this disadvantage can be mitigated by its high transmittance. As a result, we can still obtain high transmittance (>90%) at 5V, while harvesting the fast response time.

Acknowledgment

The authors are indebted to AU Optonics (AUO, Taiwan) and AFOSR for the financial supports under contract No. FA9550-14-1-0279.